PHYSICAL REVIEW D **89,** 114025 (2014)

Probing scotogenic effects in e^+e^- colliders

Shu-Yu Ho and Jusak Tandean

Department of Physics and Center for Theoretical Sciences, National Taiwan University, Taipei 106, Taiwan

(Received 13 December 2013; published 27 June 2014)

We explore the possibility of employing e^+e^- colliders to probe the scotogenic model, in which neutrinos get mass radiatively via one-loop interactions involving dark matter. Assuming the lightest one of the new particles in the model to be fermionic cold dark matter and taking into account various constraints, including those from LHC Higgs experiments, we show that LEP II data on e^+e^- scattering into a pair of charged leptons plus missing energy can place significant extra restrictions on the parameter space containing sufficiently low masses of the charged scalars in the model. On the other hand, LEP II data on e^+e^- collisions into a photon plus missing energy do not yield strong constraints. The allowed parameter space can still accommodate Higgs exotic decays into the nonstandard particles and thus is testable at the LHC. We also consider using future measurements of these two types of e^+e^- scattering at the International Linear Collider to examine the scenario of interest further and find that they can provide complementary information about it, whether or not they reveal scotogenic effects.

DOI: 10.1103/PhysRevD.89.114025 PACS numbers: 13.66.Hk, 14.60.Pq, 14.80.Bn, 95.35.+d

I. INTRODUCTION

It goes without saying that the recent observation of a Higgs boson with mass around 126 GeV at the LHC [1] and determination of the neutrino-mixing parameter $\sin\theta_{13}$ at neutrino-oscillation experiments [2] constitute crucial guideposts for attempts to establish the nature of physics beyond the standard model (SM). Another factor that any realistic scenario for new physics would need to explain is that about a quarter of the cosmic energy budget has been inferred from astronomical observations to be attributable to dark matter (DM) [3,4].

One of the most economical possibilities accommodating the essential ingredients is the scotogenic model invented by Ma [5], in which neutrinos get mass radiatively via one-loop interactions with nonstandard particles consisting of scalars and fermions, at least one of which acts as DM. Previously, within the context of this model, we have addressed [6] some of the implications of the aforementioned experimental findings, specifically the decays of the Higgs boson h into final states containing the new particles, assuming the lightest one of them to be fermionic cold DM. Taking into account various experimental and theoretical constraints, we found that such exotic decays of h could have significant rates that were already probed by existing LHC data and that the scotogenic effects on $h \to \gamma\gamma, \gamma Z$ would be testable in upcoming measurements. In the present paper, we look at additional tests on this scenario of the model using e^+e^- colliders, motivated in part by the availability of good amounts of past data from LEP II [7,8] that are potentially pertinent to our parameter space of interest and in part by the increasing prospect of the International Linear Collider (ILC) being realized in the foreseeable future [9].

The structure of the paper is as follows. In the next section, we first describe the relevant Lagrangians for the nonstandard particles in the model and the expressions related to the neutrino masses. Subsequently, adopting the Particle Data Group (PDG) parametrization of the neutrino-mixing matrix, we derive exact solutions for the Yukawa couplings of the new particles in terms of only three free parameters. We pick one set of such solutions to be used in our numerical work. In Sec. III, we briefly review the main restraints on the parameter space under consideration and also employ the Planck data on the DM relic abundance to update the allowed ranges of the Yukawa coupling belonging to the DM candidate. In Sec. IV, with the parameter values satisfying the constraints listed earlier, we investigate the scotogenic effects on the Higgs boson decay, taking into account other restrictions from the latest LHC data. Moreover, we explore complementary and further tests on the model from past measurements on e^+e^- collisions at LEP II. In particular, we show that the LEP II data on e^+e^- scattering into a pair of charged leptons plus missing energy can impose potentially important extra constraints, much more so than the data on e^+e^- colliding into a photon plus missing energy. Nevertheless, we also find that experiments on the two types of e^+e^- scattering processes at the future ILC can supply complementary results useful for probing the model. We give our conclusions in Sec. V. Some additional information and lengthy formulas are collected in a couple of appendixes.

II. INTERACTIONS AND YUKAWA COUPLINGS

In the simplest version of the scotogenic model [5,10], the components beyond the minimal SM are a scalar doublet, η, and three singlet Majorana fermions, $N_{1,2,3}$,

all of which are odd under an exactly conserved Z_2 symmetry. All of the SM particles are Z_2 even. It follows that the lightest one of the nonstandard particles is stable and can serve as DM. Here we suppose that N_1 is a good candidate for cold DM.

The Lagrangian responsible for the interactions of the scalar particles in this model with one another and with the gauge bosons is

$$\mathcal{L} = (\mathcal{D}^\rho\Phi)^\dagger\mathcal{D}_\rho\Phi + (\mathcal{D}^\rho\eta)^\dagger\mathcal{D}_\rho\eta - \mathcal{V}, \tag{1}$$

where $\mathcal{D}_\rho$ denotes the usual covariant derivative containing the SM gauge fields, the potential [5]

$$\begin{aligned}\mathcal{V} = {}& \mu_1^2\Phi^\dagger\Phi + \mu_2^2\eta^\dagger\eta + \frac{1}{2}\lambda_1(\Phi^\dagger\Phi)^2 + \frac{1}{2}\lambda_2(\eta^\dagger\eta)^2 \\ & + \lambda_3(\Phi^\dagger\Phi)(\eta^\dagger\eta) + \lambda_4(\Phi^\dagger\eta)(\eta^\dagger\Phi) \\ & + \frac{1}{2}\lambda_5[(\Phi^\dagger\eta)^2 + (\eta^\dagger\Phi)^2],\end{aligned} \tag{2}$$

and after electroweak symmetry breaking,

$$\Phi = \begin{pmatrix} 0 \\ \frac{1}{\sqrt{2}}(h+v) \end{pmatrix}, \qquad \eta = \begin{pmatrix} H^+ \\ \frac{1}{\sqrt{2}}(\mathcal{S}+i\mathcal{P}) \end{pmatrix}, \tag{3}$$

with h being the physical Higgs boson and v the vacuum expectation value (VEV) of Φ. The Z_2 symmetry implies that the VEV of η is zero. The masses of $\mathcal{S}$, $\mathcal{P}$, and $H^\pm$ are then given by

$$\begin{aligned} m_{\mathcal{S}}^2 &= m_{\mathcal{P}}^2 + \lambda_5 v^2 = \mu_2^2 + \frac{1}{2}(\lambda_3+\lambda_4+\lambda_5)v^2, \\ m_H^2 &= \mu_2^2 + \frac{1}{2}\lambda_3 v^2. \end{aligned} \tag{4}$$

We work under the assumption that λ_5 is very small [11], $|\lambda_5| \ll |\lambda_3+\lambda_4|$, implying that $m_{\mathcal{S},\mathcal{P}}$ are nearly degenerate, $|m_{\mathcal{S}}^2 - m_{\mathcal{P}}^2| = |\lambda_5|v^2 \ll m_{\mathcal{S}}^2 \simeq m_{\mathcal{P}}^2$. In $\mathcal{L}$, the part that includes the couplings of η to h, the photon A, and the Z boson is

$$\begin{aligned}\mathcal{L} \supset {}& [(\mu_2^2 - m_{\mathcal{S}}^2)\mathcal{S}^2 + (\mu_2^2 - m_{\mathcal{P}}^2)\mathcal{P}^2 + 2(\mu_2^2 - m_H^2)H^+H^-]\frac{h}{v} \\ & + ie(H^+\partial^\rho H^- - H^-\partial^\rho H^+)A_\rho + e^2H^+H^-A^2 \\ & + \frac{eg}{c_{\rm w}}(1-2s_{\rm w}^2)H^+H^-A^\rho Z_\rho + \frac{g}{2c_{\rm w}}[\mathcal{P}\partial^\rho\mathcal{S} - \mathcal{S}\partial^\rho\mathcal{P} \\ & + i(1-2s_{\rm w}^2)(H^+\partial^\rho H^- - H^-\partial^\rho H^+)]Z_\rho,\end{aligned} \tag{5}$$

where only terms pertinent to the processes we discuss are on display, $e = gs_{\rm w} > 0$ is the electromagnetic charge, and $c_{\rm w} = (1-s_{\rm w}^2)^{1/2} = \cos\theta_{\rm W}$ with the Weinberg angle $\theta_{\rm W}$.

The Lagrangian for the masses and interactions of the new singlet fermions N_k is

$$\begin{aligned}\mathcal{L}_N = {}& -\frac{1}{2}M_k\overline{N_k^{\rm c}}P_R N_k \\ & + \mathcal{Y}_{rk}\left[\bar{\ell}_r H^- - \frac{1}{\sqrt{2}}\bar{\nu}_r(\mathcal{S}-i\mathcal{P})\right]P_R N_k + {\rm H.c.},\end{aligned} \tag{6}$$

where M_k denote their masses, summation over $k, r = 1,2,3$ is implicit, the superscript c refers to charge conjugation, $P_R = \frac{1}{2}(1+\gamma_5)$, and $\ell_{1,2,3} = e, \mu, \tau$. The Yukawa couplings of N_k make up the matrix

$$\mathcal{Y} = \begin{pmatrix} Y_{e1} & Y_{e2} & Y_{e3} \\ Y_{\mu 1} & Y_{\mu 2} & Y_{\mu 3} \\ Y_{\tau 1} & Y_{\tau 2} & Y_{\tau 3} \end{pmatrix}, \tag{7}$$

where $Y_{\ell_r k} = \mathcal{Y}_{rk}$.

The light neutrinos acquire mass radiatively through one-loop diagrams with internal $\mathcal{S}$, $\mathcal{P}$, and N_k. The resulting mass eigenvalues m_j are given by [5]

$$\mathrm{diag}(m_1, m_2, m_3) = \mathcal{U}^\dagger\mathcal{M}_\nu\mathcal{U}^*, \tag{8}$$

$$\mathcal{M}_\nu = \mathcal{Y}\,\mathrm{diag}(\Lambda_1, \Lambda_2, \Lambda_3)\mathcal{Y}^{\rm T}, \tag{9}$$

$$\begin{aligned}\Lambda_k &= \frac{\lambda_5 v^2}{16\pi^2 M_k}\left[\frac{M_k^2}{m_0^2 - M_k^2} + \frac{2M_k^4\ln(M_k/m_0)}{(m_0^2 - M_k^2)^2}\right], \\ m_0^2 &= \frac{1}{2}(m_{\mathcal{S}}^2 + m_{\mathcal{P}}^2),\end{aligned} \tag{10}$$

where $\mathcal{U}$ is the Pontecorvo-Maki-Nakagawa-Sakata (PMNS [12]) unitary matrix and the formula for Λ_k applies to the $m_0 \simeq m_{\mathcal{S}} \simeq m_{\mathcal{P}}$ case.

For the $\mathcal{U}$ matrix, we choose the PDG parametrization [3]

$$\mathcal{U} = \tilde{u}\,\mathrm{diag}(e^{i\alpha_1/2}, e^{i\alpha_2/2}, 1), \tag{11}$$

$$\tilde{u} = \begin{pmatrix} c_{12}c_{13} & s_{12}c_{13} & s_{13}e^{-i\delta} \\ -s_{12}c_{23} - c_{12}s_{23}s_{13}e^{i\delta} & c_{12}c_{23} - s_{12}s_{23}s_{13}e^{i\delta} & s_{23}c_{13} \\ s_{12}s_{23} - c_{12}c_{23}s_{13}e^{i\delta} & -c_{12}s_{23} - s_{12}c_{23}s_{13}e^{i\delta} & c_{23}c_{13} \end{pmatrix}, \tag{12}$$

where $\delta \in [0, 2\pi]$ and $\alpha_{1,2} \in [0, 2\pi]$ are the Dirac and Majorana CP-violation phases, respectively, $c_{mn} = \cos\theta_{mn} \geq 0$, and $s_{mn} = \sin\theta_{mn} \geq 0$. A recent analysis of global neutrino-oscillation data yields [13][1]

$$s^2_{12} = 0.302^{+0.013}_{-0.012}, \qquad s^2_{23} = 0.413^{+0.037}_{-0.025},$$
$$s^2_{13} = 0.0227^{+0.0023}_{-0.0024}, \qquad \delta = (300^{+66}_{-138})^\circ. \tag{13}$$

Upon applying Eq. (11) in Eq. (8), we arrive at the relations

$$m_r = e^{-i\alpha_r}\sum_k X^2_{rk}\Lambda_k,$$
$$\sum_k X_{rk}X_{ok}\Lambda_k = 0, \tag{14}$$

$$X_{rk} = (\tilde{u}^\dagger \mathcal{Y})_{rk}, \qquad \alpha_3 = 0,$$
$$k, o, r = 1, 2, 3, \qquad o \neq r. \tag{15}$$

Explicitly,

$$\begin{aligned} X_{1k} &= c_{12}c_{13}Y_{ek} - \left(s_{12}c_{23} + c_{12}s_{23}s_{13}e^{-i\delta}\right)Y_{\mu k} \\ &\quad + \left(s_{12}s_{23} - c_{12}c_{23}s_{13}e^{-i\delta}\right)Y_{\tau k}, \\ X_{2k} &= s_{12}c_{13}Y_{ek} + \left(c_{12}c_{23} - s_{12}s_{23}s_{13}e^{-i\delta}\right)Y_{\mu k} \\ &\quad - \left(c_{12}s_{23} + s_{12}c_{23}s_{13}e^{-i\delta}\right)Y_{\tau k}, \\ X_{3k} &= s_{13}e^{i\delta}Y_{ek} + s_{23}c_{13}Y_{\mu k} + c_{23}c_{13}Y_{\tau k}. \end{aligned} \tag{16}$$

The diagonalization conditions in Eq. (14) turn out to be exactly solvable for two of the three elements $Y_{\ell_r k}$ with the same k in terms of the third one, in which case the $\mathcal{Y}$ matrix has only three free (complex) parameters. We opt for getting Y_{ek} and $Y_{\mu k}$ in terms of $Y_k \equiv Y_{\tau k}$. As outlined in Appendix A, there is more than one set of the solutions, but not all of the sets fulfill the requirement that at least two of the mass eigenvalues $m_{1,2,3}$ be nonzero.

One of the solution sets that can supply three nonzero masses of the neutrinos comprises

$$\begin{aligned} Y_{e1} &= \frac{-c_{12}c_{13}Y_1}{c_{12}c_{23}s_{13}e^{i\delta} - s_{12}s_{23}}, \\ Y_{\mu 1} &= \frac{c_{12}s_{23}s_{13}e^{i\delta} + s_{12}c_{23}}{c_{12}c_{23}s_{13}e^{i\delta} - s_{12}s_{23}}Y_1, \\ Y_{e2} &= \frac{-s_{12}c_{13}Y_2}{s_{12}c_{23}s_{13}e^{i\delta} + c_{12}s_{23}}, \\ Y_{\mu 2} &= \frac{s_{12}s_{23}s_{13}e^{i\delta} - c_{12}c_{23}}{s_{12}c_{23}s_{13}e^{i\delta} + c_{12}s_{23}}Y_2, \\ Y_{e3} &= \frac{s_{13}Y_3}{c_{23}c_{13}e^{i\delta}}, \qquad Y_{\mu 3} = \frac{s_{23}Y_3}{c_{23}}, \end{aligned} \tag{17}$$

which correspond to the mass eigenvalues

$$m_1 = \frac{\Lambda_1 Y^2_{e1}e^{-i\alpha_1}}{c^2_{12}c^2_{13}}, \qquad m_2 = \frac{\Lambda_2 Y^2_{e2}e^{-i\alpha_2}}{s^2_{12}c^2_{13}}, \qquad m_3 = \frac{\Lambda_3 Y^2_3}{c^2_{13}c^2_{23}}. \tag{18}$$

The necessity that $m_{1,2,3}$ be real and nonnegative then implies that

$$\alpha_1 = \arg(\Lambda_1 Y^2_{e1}), \qquad \alpha_2 = \arg(\Lambda_2 Y^2_{e2}), \qquad \arg(\Lambda_3 Y^2_3) = 0. \tag{19}$$

In the rest of the paper, we utilize Eqs. (17) and (18), and for simplicity, we set $e^{i\delta} = 1$, in accord with the empirical range of δ in Eq. (13). Also, we take $Y_{1,2,3}$ to be real and nonnegative.

Now, in our previous study, we adopted a simpler form of $\mathcal{U}$, which depends on only two angles, θ and ς, and has no phases [6]. It can be reproduced from $\tilde{u}$ in Eq. (11) with

$$s_{12} = \frac{s_\theta}{\sqrt{1 - c^2_\theta s^2_\varsigma}}, \qquad s_{23} = \frac{c_\varsigma - s_\theta s_\varsigma}{\sqrt{2 - 2c^2_\theta s^2_\varsigma}}, \qquad s_{13} = c_\theta s_\varsigma, \tag{20}$$

and $\delta = 0$, where $c_a = \cos a$ and $s_a = \sin a$. Moreover, numerically, we chose for definiteness $\theta = 32.89^\circ$ and $c_\theta s_\varsigma = \sqrt{0.0227}$, which led to $\mathcal{U}$ elements in agreement at the one-sigma level with their experimental values in Eq. (13). Hence, in the present analysis, we adopt for $\tilde{u}$ the same numerical input. According to Eq. (20), this translates into $s^2_{12} \simeq 0.302$, $s^2_{23} \simeq 0.402$, and $s^2_{13} = 0.0227$, consistent with Eq. (13) and leading to the neutrino eigenmasses[2]

$$m_1 \simeq 15.9\Lambda_1 Y^2_1, \qquad m_2 \simeq 2.8\Lambda_2 Y^2_2, \qquad m_2 \simeq 1.7\Lambda_3 Y^2_3. \tag{21}$$

[1]Somewhat earlier analyses of the global neutrino data in Ref. [14] produced similar results.

[2]It is instructive to see how $m_{1,2,3}$ would be modified with a tribimaximal form [15] of the mixing matrix $\mathcal{U}$, which corresponds to $(s^2_{12}, s^2_{23}, s^2_{13}) = (1/3, 1/2, 0)$ and is therefore no longer compatible with the current data [13]. Applying this to Eq. (18), with zero phases, yields $(m_1, m_2, m_3) = (6\Lambda_1 Y^2_1, 3\Lambda_2 Y^2_2, 2\Lambda_3 Y^2_3)$ [16]. Hence, the m_1 value is very different from that in Eq. (21).

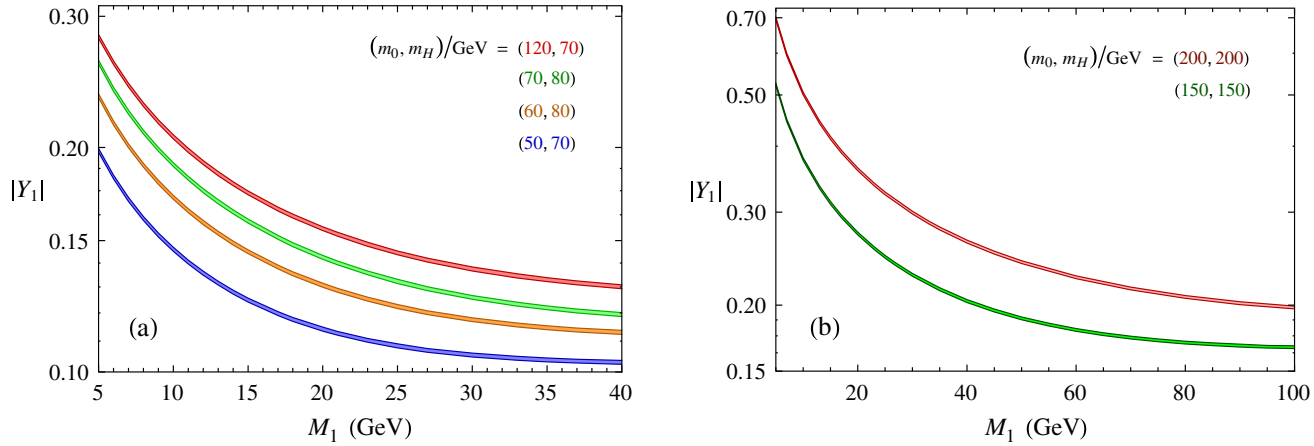

FIG. 1 (color online). Sample values of Yukawa parameter $|Y_1|$ over two different ranges of N_1 mass, M_1, fulfilling the relic density requirement for some selections of the new neutral and changed scalars' masses (m_0, m_H).

III. CONSTRAINTS FROM LOW ENERGY AND DM DATA

As we discussed in Ref. [6], there are a number of theoretical and experimental restrictions on the couplings and masses of the nonstandard particles in the scotogenic scenario being examined. We found specifically that the strictest limitations on the Yukawa couplings $\mathcal{Y}_{rk}$ come from the data on the neutrino squared-mass differences $\Delta^2_{jk} = m^2_j - m^2_k$, the empirical bounds on the branching ratios of the charged-lepton flavor-changing radiative decays $\ell_i \to \ell_j \gamma$, and the measurement of the muon anomalous magnetic moment a_μ. The parameter space of interest in this study is subject to the same restraints from low-energy experiments.

Also important are constraints on $\mathcal{Y}_{r1} \propto Y_1$ from the observed DM relic abundance, Ω, as we have selected N_1 to be the lightest of the nonstandard particles and play the role of cold DM. The dominant contributions to Ω arise from the N_1 annihilations into $\nu_i \nu_j$ and $\ell_i^- \ell_j^+$, which are induced at tree level by $(\mathcal{S}, \mathcal{P})$ and $H^\pm$ exchanges, respectively. Each of them involves diagrams in the t and u channels because of the Majorana nature of the external neutral fermions. In Ref. [6], we derived the amplitudes for $N_1 N_1 \to \nu_i \nu_j, \ell_i^- \ell_j^+$ and computed the corresponding annihilation rate in order to extract the values of $|Y_1|$ consistent with the Ω data supplied by the PDG. Here we update the allowed ranges of $|Y_1|$ by demanding it to satisfy instead $0.1159 \le \Omega \hat{h}^2 \le 0.1215$, where $\hat{h}$ is the Hubble constant. This is the 90% confidence level range of $\Omega \hat{h}^2 = 0.1187 \pm 0.0017$, which was determined by the Planck Collaboration [4] from the Planck measurement and other data. We display in Fig. 1(a) some examples of the resulting $|Y_1|$ over $5\ \text{GeV} \le M_1 \le 40\ \text{GeV}$ for the solutions in Eq. (17) and different sets of $m_0 \simeq m_\mathcal{S} \simeq m_\mathcal{P}$ and m_H. The allowed ranges of $|Y_1|$ in this plot are narrower than those found in Ref. [6] using the less precise PDG number for Ω. In Fig. 1(b), we present examples for a larger range of M_1 which may be probed at high-energy electron-positron colliders. More details on the various constraints mentioned only briefly in this section are available in Ref. [6].

IV. SCOTOGENIC EFFECTS IN HIGGS DECAY AND e^+e^- COLLISIONS

For the M_1 range shown in Fig. 1(a), the appropriate values of $M_{2,3} > M_1$, and sufficiently low masses of the new scalars, $m_{0,H}$, the Higgs boson h may decay into final states involving the nonstandard particles. In Ref. [6], we considered such decays which proceed from tree-level diagrams, namely $h \to \mathcal{S}\mathcal{S}(\mathcal{P}\mathcal{P})$ or $h \to \nu_r N_k \mathcal{S}(\mathcal{P})$, $H^\pm \ell_r^\mp N_k$, depending on the daughter particles' masses, over the regions $50\ \text{GeV} \le m_0 \le 120\ \text{GeV}$ and $70\ \text{GeV} \le m_H \le 120\ \text{GeV}$. As we found previously, these exotic decay channels are allowed to have enhanced rates by the constraints described in the preceding section, including the updated one from the Planck data. We list several instances of this in the tenth column of Table I for different sets of the mass parameters $m_{0,H}$, μ_2, and $M_{1,2,3}$. For this table, we have employed the Higgs mass $m_h = 125.5\ \text{GeV}$, compatible with the latest measurements [17,18], and the SM Higgs total width $\Gamma_h^{\text{SM}} = 4.14\ \text{MeV}$ [19]. The branching ratio $\mathcal{B}_{\mathcal{S}\mathcal{P}H} = \Gamma_{\mathcal{S}\mathcal{P}H}/(\Gamma_h^{\text{SM}} + \Gamma_{\mathcal{S}\mathcal{P}H})$ involves the combined rate $\Gamma_{\mathcal{S}\mathcal{P}H}$ of all of the kinematically permitted exotic modes mentioned above [6]. The two numbers on each line under $\mathcal{B}_{\mathcal{S}\mathcal{P}H}$ correspond to the two different numbers on the same line in the μ_2 column, which includes the possibility that μ_2^2 can be negative [20]. In the last four rows, $\mathcal{B}_{\mathcal{S}\mathcal{P}H} = 0$ because these exotic decays of the Higgs cannot happen for the large mass choices.

The last two columns in Table I illustrate the impact of the new particles on the standard decay channels $h \to \gamma\gamma$ and $h \to \gamma Z$. These decays are of great interest because they arise from loop diagrams and hence are sensitive to possible new-physics contributions, which are $H^\pm$ in our case.

TABLE I. Sample values of mass parameters $m_{0,H}$, μ_2, and $M_{1,2,3}$, and Yukawa constants $Y_{1,2,3}$ satisfying the constraints discussed in Sec. III and the resulting branching ratios $\mathcal{B}_{\mathcal{SP}H}$ of the Higgs decay into final states containing $\mathcal{S}, \mathcal{P}$, or $H^\pm$ and ratios $\mathcal{R}_{\gamma\mathcal{V}^0}$ of $\Gamma(h \to \gamma\mathcal{V}^0)$ to its SM value for $\mathcal{V}^0 = \gamma, Z$.

$\frac{m_0}{\text{GeV}}$	$\frac{m_H}{\text{GeV}}$	$\frac{\mu_2}{\text{GeV}}$	$\frac{M_1}{\text{GeV}}$	$\frac{M_2}{\text{GeV}}$	$\frac{M_3}{\text{GeV}}$	Y_1	Y_2	Y_3	$\mathcal{B}_{\mathcal{SP}H}$ (%)	$\mathcal{R}_{\gamma\gamma}$	$\mathcal{R}_{\gamma Z}$
50	70	46 (47)	9	14	64	0.152	0.363	0.642	20 (14)	0.89 (0.89)	0.95 (0.95)
60	80	54 (56)	10	15	72	0.171	0.410	0.703	26 (14)	0.91 (0.92)	0.96 (0.97)
70	80	113 ($7i$)	12	18	79	0.175	0.422	0.740	24 (12)	1.2 (0.84)	1.1 (0.93)
120	70	123 (111)	20	29	85	0.155	0.380	0.712	20 (12)	1.5 (1.3)	1.2 (1.1)
50	85	54 (53)	35	51	143	0.107	0.262	0.603	21 (13)	0.91 (0.91)	0.96 (0.96)
50	90	46 (47)	30	43	125	0.110	0.264	0.575	18 (11)	0.90 (0.90)	0.96 (0.96)
65	90	140 ($70i$)	40	57	153	0.119	0.293	0.658	25 (11)	1.2 (0.79)	1.1 (0.91)
70	85	199 ($135i$)	50	71	178	0.119	0.300	0.707	0.6 (0.3)	1.8 (0.54)	1.3 (0.80)
150	150	80 (280)	50	72	181	0.188	0.452	0.917	0 (0)	0.92 (1.3)	0.97 (1.1)
150	150	90 (290)	100	142	277	0.167	0.415	0.947	0 (0)	0.93 (1.3)	0.97 (1.1)
200	200	80 (330)	50	75	220	0.241	0.578	1.131	0 (0)	0.91 (1.2)	0.97 (1.1)
200	200	70 (340)	100	143	265	0.199	0.477	1.027	0 (0)	0.91 (1.2)	0.97 (1.1)

Furthermore, these channels are already under investigation at the LHC [17,18,21]. The ratios $\mathcal{R}_{\gamma\mathcal{V}^0} = \Gamma(h \to \gamma\mathcal{V}^0)/\Gamma(h \to \gamma\mathcal{V}^0)_{\text{SM}}$ for $\mathcal{V}^0 = \gamma, Z$ would thus signal new physics if they are unambiguously measured to deviate from unity.

The predictions for $\mathcal{B}_{\mathcal{SP}H}$ and $\mathcal{R}_{\gamma\gamma}$ in Table I can already be tested experimentally. Recent analyses [22] have determined that the present Higgs data allow the branching ratio of its nonstandard decays into invisible or undetected final states to reach 22% at the 95% confidence level if the Higgs production mechanism is SM-like, which is the case in the scotogenic model. This restriction is not yet severe for $\mathcal{B}_{\mathcal{SP}H}$ and can be readily avoided by changing μ_2, as can be viewed in the table. For $h \to \gamma\gamma$, which has been detected, unlike the γZ channel [21], the prediction can be compared to observation. The measurements of the signal strength for $h \to \gamma\gamma$ by the ATLAS and CMS Collaborations are $\sigma/\sigma_{\text{SM}} = 1.55^{+0.33}_{-0.28}$ [17] and $\sigma/\sigma_{\text{SM}} = 0.77 \pm 0.27$ [18], respectively. Evidently, the majority of the $\mathcal{R}_{\gamma\gamma}$ numbers are in agreement with one or the other of these LHC results. Pending an experimental consensus on this decay mode and the advent of complementary information from the future detection of $h \to \gamma Z$, we are motivated to pursue other means to probe the model to a greater degree.

The new sector of the model being leptophilic, one may want to look into extra tests on it by means of electron-positron scattering. Below we demonstrate that potentially significant restraints on the model are indeed available from past measurements at LEP II. Since the ILC may become a reality in the not too distant future, providing e^+e^- scattering experiments at higher energies and with better precision, we also make some estimates and comments relevant to it. In the rest of this section, we focus on scotogenic contributions to e^+e^- collisions into a pair of charged leptons plus missing energy and into a photon plus missing energy.

A. $e^+e^- \to H^+H^- \to \ell^+\ell'^-\not{E}$

The amplitude for $e^+(p_+)e^-(p_-) \to H^+(q_+)H^-(q_-)$, which comes from γ- and Z-mediated diagrams in the s channel and N_k-mediated diagrams in the t channel, follows from Eqs. (5) and (6). It can be expressed as

$$\mathcal{M}_{e\bar{e}\to H\bar{H}} = \frac{-2e^2\bar{v}_{e^+}\not{q}_- u_{e^-}}{s} - \frac{2\bar{v}_{e^+}\not{q}_-(g_L^2 P_L + g_L g_R P_R)u_{e^-}}{s - m_Z^2 + i\Gamma_Z m_Z} + \sum_k \frac{|\mathcal{Y}_{1k}|^2 \bar{v}_{e^+}\not{q}_- P_L u_{e^-}}{M_k^2 - t}, \tag{22}$$

where u_e and v_e are Dirac spinors, $s = (p_+ + p_-)^2$, $t = (p_+ - q_+)^2$, $g_L = g(s_{\text{w}}^2 - 1/2)/c_{\text{w}}$, $g_R = g s_{\text{w}}^2/c_{\text{w}}$, and $P_L = \frac{1}{2}(1 - \gamma_5)$. We have relegated the resulting cross section, $\sigma_{e\bar{e}\to H\bar{H}}$, to Eq. (B1) in Appendix B.

After their production, $H^\pm$ will decay into $\ell_o^\pm N_k$ if $m_H > m_{\ell_o} + M_k$. For $k = 2$ or 3, the decays $N_k \to \ell_r^\pm H^\mp$ and $N_k \to \nu\mathcal{S}, \nu\mathcal{P}$ may occur, followed, respectively, by $H^\pm \to \ell_s^\pm N_l$ if $m_H > m_{\ell_s} + M_l$ and $\mathcal{S}, \mathcal{P} \to \nu N_l$. If these two-body channels of N_k are not open, it will instead undergo $N_k \to \nu_o\nu_r N_l$ and possibly $N_k \to \ell_o^-\ell_r^+ N_l$. We have collected the expressions for the rates of these various decays of $H^\pm$, $\mathcal{S}$, $\mathcal{P}$, and N_k in Appendix B.[3] In the final states of the decays just mentioned, N_l will no longer decay if $l = 1$.

Thus, since N_1 is DM, the channel $e^+e^- \to \ell^+\ell'^-\not{E}$ with missing energy $\not{E}$ in the final state receives the scotogenic contribution $e^+e^- \to H^+H^- \to \ell^+\ell'^-\not{E}$. We can write its cross section as

[3]In this paper, we do not consider scenarios with $|m_H - m_{\mathcal{S},\mathcal{P}}| \geq m_{W,Z}$, in which the new scalars may also be detectable through other two-body decays, like $H^\pm \to \mathcal{S}(\mathcal{P})W^\pm$. Such a possibility has been discussed in the context of the inert doublet model [23,24] without N_k.

$$\sigma_{e\bar{e}\to H\bar{H}\to\ell\bar{\ell}'\not{E}} = \sigma_{e\bar{e}\to H\bar{H}}\left(\sum_r \mathcal{B}(H\to\ell_r\not{E})\right)^2 \qquad (23)$$

with the branching ratios

$$\begin{aligned}\mathcal{B}(H\to\ell_r\not{E}) &= \mathcal{B}(H\to\ell_r N_1) + \mathcal{B}(H\to\ell_r N_2)\mathcal{B}_{21} \\ &\quad + \mathcal{B}(H\to\ell_r N_3)\mathcal{B}_{31}, \\ \mathcal{B}_{21} &= \mathcal{B}(N_2\to\nu\nu' N_1), \\ \mathcal{B}_{31} &= \mathcal{B}(N_3\to\nu\nu' N_1) + \mathcal{B}(N_3\to\nu\nu' N_2)\mathcal{B}_{21}, \end{aligned} \qquad (24)$$

where $\mathcal{B}(N_k\to\nu\nu' N_l) = \sum_{\hat{\eta}=\mathcal{S},\mathcal{P}}(\Gamma_{N_k\to\nu\hat{\eta}}/\Gamma_{N_k})\Gamma_{\hat{\eta}\to\nu N_l}/\Gamma_{\hat{\eta}}$ or $\Gamma_{N_k\to\nu\nu' N_l}/\Gamma_{N_k}$ depending on the masses. Any of the terms in $\mathcal{B}(H\to\ell_r\not{E})$ would be absent if kinematically forbidden.

Since according to Eq. (5) the Z boson can couple to $\mathcal{S}$ and $\mathcal{P}$, it can mediate $e^+e^-\to\mathcal{S}\mathcal{P}$ in the s channel. This transition is experimentally unobservable if $\mathcal{S}$ and $\mathcal{P}$ each decay (sequentially) into an N_1 along with one or more νs, as all of these fermions are invisible.[4] On the other hand, if only one member of the $\mathcal{S}\mathcal{P}$ pair undergoes such a decay, while the other member decays into $\ell^+\ell'^-N_1$ and one or more νs, then $e^+e^-\to\mathcal{S}\mathcal{P}$ will also contribute to the $\ell^+\ell'^-\not{E}$ final state. With $m_\mathcal{S}\simeq m_\mathcal{P}\simeq m_0$, we can write the cross section of this contribution as $\sigma_{e\bar{e}\to\mathcal{S}\mathcal{P}\to\ell\bar{\ell}'\not{E}} = 2\sigma_{e\bar{e}\to\mathcal{S}\mathcal{P}}\mathcal{B}(\hat{\eta}\to\not{E})\mathcal{B}(\hat{\eta}\to\ell\bar{\ell}'\not{E})$, where $\sigma_{e\bar{e}\to\mathcal{S}\mathcal{P}}$ is given in Appendix B for completeness, $\hat{\eta}=\mathcal{S}$ or $\mathcal{P}$, $\mathcal{B}(\hat{\eta}\to\not{E})=\mathcal{B}(\hat{\eta}\to\nu N_1)+\mathcal{B}(\hat{\eta}\to\nu N_2)\mathcal{B}_{21}+\mathcal{B}(\hat{\eta}\to\nu N_3)\mathcal{B}_{31}$, and $\mathcal{B}(\hat{\eta}\to\ell\bar{\ell}'\not{E}) = \mathcal{B}(\hat{\eta}\to\nu N_2)\mathcal{B}(N_2\to\ell\bar{\ell}'\not{E}) + \mathcal{B}(\hat{\eta}\to\nu N_3)\mathcal{B}(N_3\to\ell\bar{\ell}'\not{E})$. Having more powers of the branching ratios, $\sigma_{e\bar{e}\to\mathcal{S}\mathcal{P}\to\ell\bar{\ell}'\not{E}}$ can be expected to be suppressed with respect to $\sigma_{e\bar{e}\to H\bar{H}\to\ell\bar{\ell}'\not{E}}$. This turns out to be the case for the parameter choices in our illustrations, the suppression factors being a few or more. The impact of $\sigma_{e\bar{e}\to\mathcal{S}\mathcal{P}\to\ell\bar{\ell}'\not{E}}$ on $\sigma_{e\bar{e}\to H\bar{H}\to\ell\bar{\ell}'\not{E}}$ is actually further subdued because the angular distributions of the final lepton pairs, $\ell^+\ell'^-$, in the two processes are generally very different. For these reasons, hereafter we neglect the effect of $e^+e^-\to\mathcal{S}\mathcal{P}\to\ell^+\ell'^-\not{E}$ in examining $e^+e^-\to H^+H^-\to\ell^+\ell'^-\not{E}$.

The process $e^+e^-\to\ell^+\ell'^-\not{E}$ with the final charged leptons not originating from the same particle has been well measured at LEP II [7]. The experimental values of its cross section at center-of-mass (c.m.) energies $\sqrt{s}\simeq$ 183–208 GeV vary from about 1.4 to 2.5 pb with errors ranging mostly between 10% and 20%. Except for several of them, the measurements are consistent at the one-sigma level with the SM prediction for $e^+e^-\to W^+W^-\to\nu\nu'\ell^+\ell'^-$, summed over all of the final leptons. Accordingly, we may demand that $\sigma_{e\bar{e}\to H\bar{H}\to\ell\bar{\ell}'\not{E}} < 0.3$ pb.

To get some indications as to which of the examples in Table I can meet this condition, we present the cross sections in Table II at the c.m. energies $\sqrt{s} = 183, 196, 207$ GeV representing the LEP II range. Obviously the parameter values yielding the cross sections at these energies in the first four rows are disfavored by the LEP II data. In contrast, the corresponding numbers in the second four rows can fulfill the imposed bound due to the relatively larger m_H and M_k and smaller Y_k. Interestingly, in these latter examples, the Higgs exotic decays into the scotogenic particles can mostly still happen with nonnegligible rates, as illustrated by their $\mathcal{B}_{\mathcal{S}\mathcal{P}H}$ entries in the second four rows of Table I.

For the parameter space that can evade the LEP II restrictions and has room for the scotogenic decays of the Higgs compatible with LHC data, further tests are potentially available at a future higher energy e^+e^- collider, such as the ILC [9]. Moreover, $H^\pm$ which are too heavy to have been produced at LEP II may be within the reach of the ILC.[5] The last three columns of Table II show a number of predictions for $\sigma_{e\bar{e}\to H\bar{H}\to\ell\bar{\ell}'\not{E}}$ at some of the proposed ILC energies. The predictions are to be compared with the SM cross sections

$$\sigma_{e\bar{e}\to W\bar{W}\to\nu\nu'\ell\bar{\ell}'} = 1.7, 0.8, 0.3 \text{ pb}, \qquad (25)$$

which are the tree-level values at $\sqrt{s} = 250, 500,$ 1000 GeV, respectively. Since the scotogenic contributions are of roughly similar order to, or substantially exceed, the SM ones, we can conclude that experiments on $e^+e^-\to\ell^+\ell'^-\not{E}$ at the ILC have the potential to discover scotogenic signals or impose stringent limits on the parameter regions examined in this paper.

Once $H^\pm$ are discovered, precise measurements on their decay modes, especially $H^\pm\to\ell_r^\pm N_k$, will help uncover the flavor structure of the Yukawa interactions of the new particles. Specifically, as Eq. (B4) indicates, ratios of the magnitudes of Yukawa couplings $\mathcal{Y}_{rk}$ can be inferred from the ratios of the experimental branching ratios of these two-body decays. At e^+e^- colliders, such ratios can be measured after sufficient data are accumulated to allow the identification of the lepton flavors in the $\ell^+\ell'^-\not{E}$ signal events. However, it may be difficult to extract clearly the individual $|\mathcal{Y}_{rk}|$ themselves because $e^+e^-\to H^+H^-$ is induced not only by γ- and Z-mediated diagrams, but also by N_k-mediated diagrams which involve $\mathcal{Y}_{1k}$. On the other hand, at the LHC, both the relative and absolute values of $|\mathcal{Y}_{rk}|$ are measurable if enough statistics are available, as the main production channel is the quark annihilation $q\bar{q}\to H^+H^-$ via γ and Z exchanges only. The acquired data on $H^\pm\to\ell_r^\pm N_k$ will, in addition, reveal the masses of N_k. All of this information on $\mathcal{Y}_{rk}$ and M_k, plus the masses of the new scalars, is crucial because they also determine the light

[4]Without observable events, due to the absence of detectable particles in the final state, an empirical cross section would not be available to check the theory [25,26].

[5]The potential reach of the ILC to measure $e^+e^-\to H^+H^-$ in the inert doublet model [20,23] without N_k, or in the scotogenic model with $\mathcal{S}$ being the DM candidate and N_k very heavy, has recently been studied in Ref. [24].

TABLE II. Cross section of $e^+e^- \to H^+H^- \to \ell^+\ell'^-\not{E}$ corresponding to the examples in Table I for c.m. energies $\sqrt{s} = 183, 196, 207, 250, 500, 1000$ GeV, with both $H^\pm$ being on shell.

$\frac{m_0}{\text{GeV}}$	$\frac{m_H}{\text{GeV}}$	$\frac{M_1}{\text{GeV}}$	$\frac{M_2}{\text{GeV}}$	$\frac{M_3}{\text{GeV}}$	Y_1	Y_2	Y_3	$\sigma_{e\bar{e}\to H\bar{H}\to\ell\bar{\ell}'\not{E}}$ (pb) 183	196	207	250	500	1000
50	70	9	14	64	0.152	0.363	0.642	4.0	4.8	5.3	6.2	3.8	1.4
60	80	10	15	72	0.171	0.410	0.703	2.5	3.9	5.0	7.2	5.5	2.1
70	80	12	18	79	0.175	0.422	0.740	2.3	3.7	4.7	6.8	5.0	1.9
120	70	20	29	85	0.155	0.380	0.712	1.4	1.7	1.9	2.2	1.3	0.49
50	85	35	51	143	0.107	0.262	0.603	0.06	0.16	0.24	0.49	0.52	0.24
50	90	30	43	125	0.110	0.264	0.575	0.01	0.10	0.19	0.51	0.61	0.27
65	90	40	57	153	0.119	0.293	0.658	0.01	0.12	0.23	0.59	0.71	0.33
70	85	50	71	178	0.119	0.300	0.707	0.08	0.19	0.29	0.57	0.66	0.32
150	150	50	72	181	0.188	0.452	0.917	0	0	0	0	1.8	1.2
150	150	100	142	277	0.167	0.415	0.947	0	0	0	0	0.96	0.76
200	200	50	75	220	0.241	0.578	1.131	0	0	0	0	2.0	2.8
200	200	100	143	265	0.199	0.477	1.027	0	0	0	0	0.69	1.1

neutrinos' mass matrix and the rates of the flavor-changing decays $\ell_o \to \ell_r\gamma$, as well as the relic density of the DM particle N_1. In other words, a good amount of experimental data on the various quantities which are functions of $\mathcal{Y}_{rk}$ and the new particles' masses will serve to check the predictions, and hence, the self-consistency, of the model.[6]

B. $e^+e^- \to \gamma NN', \gamma\mathcal{SP} \to \gamma\not{E}$

Another kind of scotogenic effect that may be observable at e^+e^- colliders is $e^+e^- \to \gamma N_j N_k$, which, if $j, k > 1$, is followed by $N_{j,k}$ decaying (sequentially) into N_1 plus light neutrinos. This is generated by H-exchange diagrams with the photon radiated off the $e^\pm$ lines. We have written down the scattering amplitude, which depends on $\mathcal{Y}_{1j,1k}$, and sketched the calculation of the cross section, $\sigma_{e\bar{e}\to\gamma N_j N_k}$, in Appendix B. In view of the Majorana nature of $N_{j,k}$, we can express its contribution to the monophoton production process $e^+e^- \to \gamma\not{E}$ as

$$\sigma_{e\bar{e}\to\gamma NN'\to\gamma\not{E}} = \sum_{\substack{j,k=1\\ j\le k}}^{3} \sigma_{e\bar{e}\to\gamma N_j N_k}\mathcal{B}_{j1}\mathcal{B}_{k1}, \qquad (26)$$

where $\mathcal{B}_{21,31}$ are defined in Eq. (24) and $\mathcal{B}_{11} = 1$. Any of the terms in this sum would vanish if kinematically forbidden.

There is an additional scotogenic contribution to $e^+e^- \to \gamma\not{E}$, namely $e^+e^- \to \gamma\mathcal{SP}$ induced by Z-mediated diagrams with the photon being emitted from the $e^\pm$ legs. We have outlined the computation of its cross section, $\sigma_{e\bar{e}\to\gamma\mathcal{SP}}$, in Appendix B. The $\gamma\not{E}$ final state is reached when $\mathcal{S}$ and $\mathcal{P}$ each decay (sequentially) into N_1 and one or more light neutrinos. Putting things together, we arrive at the cross section

$$\sigma_{e\bar{e}\to\gamma\mathcal{SP}\to\gamma\not{E}} = \sigma_{e\bar{e}\to\gamma\mathcal{SP}}(\mathcal{B}(\hat{\eta}\to\not{E}))^2, \qquad (27)$$

with the branching ratio $\mathcal{B}(\hat{\eta}\to\not{E}) = \mathcal{B}(\hat{\eta}\to\nu N_1) + \mathcal{B}(\hat{\eta}\to\nu N_2)\mathcal{B}_{21} + \mathcal{B}(\hat{\eta}\to\nu N_3)\mathcal{B}_{31}$. As it turns out, $\sigma_{e\bar{e}\to\gamma\mathcal{SP}\to\gamma\not{E}}$ is numerically less important than $\sigma_{e\bar{e}\to\gamma NN'\to\gamma\not{E}}$ for the mass and coupling values in our examples.

Much experimental work on $e^+e^- \to \gamma\not{E}$ has also been performed at LEP II to study the neutrino counting reaction $e^+e^- \to \gamma\nu\bar{\nu}$ in the SM and also to search for long-lived or stable new particles [8]. The measured cross sections at $\sqrt{s} \simeq 130$–207 GeV, with errors mainly between 5% and 20%, vary not only with $\sqrt{s}$, but also with the experimental cuts on the photon energy E_γ and angle θ_γ relative to the beam direction. From a collection of these data [8] tabulated in Ref. [29], one can see that the experimental and SM values of the cross section agree with each other at the one-sigma level, except for several of them.

Comparing with the LEP II results on $e^+e^- \to \gamma\not{E}$, we find that for the parameter ranges that escape the bounds from $e^+e^- \to \ell^+\ell'^-\not{E}$ data discussed in the previous subsection the scotogenic contributions to $e^+e^- \to \gamma\not{E}$ at LEP II energies do not yield significant effects. The scotogenic contributions are even small compared to the experimental errors. Consequently, we need to turn to the ILC in order to explore the possibility of seeing the desired signals.[7]

After appropriate cuts on the photon energy and angle are imposed, the main background is $e^+e^- \to \gamma\nu\bar{\nu}$ in the

[6]Much of the discussion in this paragraph also applies to some other scenarios of one-loop radiative neutrino mass in which the neutrino and DM sectors are intimately connected, such as the model proposed in Ref. [27]. Its LHC phenomenology is the focus of Ref. [28], which provides a detailed analysis on the possibility of searching for a signal in $\ell^+\ell'^-\not{E}$ final states.

[7]Similar situations may arise in some other radiative neutrino mass models with fermionic DM [30,31] and more generally in models with nonnegligible effective DM-electron couplings [26].

TABLE III. Cross section of $e^+e^- \to \gamma NN', \gamma\mathcal{S}\mathcal{P} \to \gamma\not{E}$, in fb, for the parameter values in some of the examples in Table II at c.m. energies $\sqrt{s} = 250, 500, 1000$ GeV. The two terms in each of the sums correspond to the $\gamma NN'$ and $\gamma\mathcal{S}\mathcal{P}$ contributions, respectively. The cuts applied to the photon energy and angle relative to the incident electron's direction are $E_\gamma \sin\theta_\gamma \geq 0.15\sqrt{s}$ and $|\cos\theta_\gamma| \leq 0.7$, as well as $E_\gamma \leq \min(0.45\sqrt{s}, E_\gamma^{\max})$, where $E_\gamma^{\max}$ is related to the $N_{k,l}$ $[\mathcal{S}, \mathcal{P}]$ masses by Eq. (B18) [Eq. (B22)]. In the bottom row are the corresponding numbers for $e^+e^- \to \gamma\nu\bar{\nu}$ in the SM, with the same cuts except $E_\gamma \leq 0.45\sqrt{s}$.

$\frac{m_0}{\text{GeV}}$	$\frac{m_H}{\text{GeV}}$	$\frac{M_1}{\text{GeV}}$	$\frac{M_2}{\text{GeV}}$	$\frac{M_3}{\text{GeV}}$	Y_1	Y_2	Y_3	$\sigma_{e\bar{e}\to\gamma NN',\gamma\mathcal{S}\mathcal{P}\to\gamma\not{E}}$ (fb) 250	500	1000
65	90	40	57	153	0.119	0.293	0.658	$3.3 + 0.76$	$2.5 + 0.48$	$1.0 + 0.14$
70	85	50	71	178	0.119	0.300	0.707	$2.7 + 0.54$	$2.7 + 0.46$	$1.1 + 0.14$
150	150	50	72	181	0.188	0.452	0.917	$4.7 + 0$	$6.7 + 0.04$	$3.5 + 0.06$
200	200	50	75	220	0.241	0.578	1.131	$6.3 + 0$	$12.2 + 0.00$	$7.6 + 0.03$
$\sigma^{\text{SM}}_{e\bar{e}\to\gamma\nu\bar{\nu}}$ (fb)								613	95.5	61.1

SM, which can be calculated with formulas available in the literature [29,32]. Among the examples in Table II, we obtain a few that produce contributions to $e^+e^- \to \gamma\not{E}$, which are not negligible compared to the background at ILC energies. We display the results in Table III where the cuts used are specified. The entries for $\sqrt{s} = 250, 500, 1000$ GeV are to be compared to the SM numbers in the bottom row. Although the cross sections of $e^+e^- \to \gamma NN', \gamma\mathcal{S}\mathcal{P} \to \gamma\not{E}$ in the first two rows are below 4% of the background, the ones in the next two rows can reach about 7% to 13%, notably at $\sqrt{s} = 500, 1000$ GeV. Assuming that the proposed integrated luminosities of 500 and 1000 fb^{-1} at these energies [9], respectively, are achievable, we may expect that there will be enough events to distinguish signals from backgrounds. If that is the case, then these examples have illustrated that the information to be gained from the ILC data on $e^+e^- \to \gamma\not{E}$ is complementary to that from $e^+e^- \to \ell^+\ell'^-\not{E}$ in probing the scotogenic model further. Especially, if a new-physics hint is detected in the $\ell^+\ell'^-\not{E}$ events, the $\gamma\not{E}$ measurement could serve to offer some cross-checks, but the observation of a nonstandard signal in only the $\gamma\not{E}$ data would likely disfavor the scenario discussed above.

V. CONCLUSIONS

We have investigated the possibility of employing e^+e^- colliders to provide additional tests on the scotogenic model of radiative neutrino mass. This study continues our previous work which addressed the Higgs boson undergoing exotic decays into the nonstandard particles of the same model. Unlike before, here we adopt the PDG parametrization of the neutrino-mixing matrix and derive exact solutions for the Yukawa couplings of the new particles in terms of three free (complex) parameters. Accordingly, the Yukawa results are consistent with the measured elements of the mixing matrix. We select one set of such solutions to be used in our numerical computation. As before, we assume that the lightest one of the new fermions is the cold DM candidate. Then, taking into account various theoretical and experimental constraints, including those from low-energy measurements and the Planck data on the relic DM density, we scan the model parameter space for regions that can accommodate the Higgs exotic decays and also masses of the new particles that can be produced at e^+e^- colliders. At present, the LHC Higgs data do not yet translate into severe restrictions on the allowed parameter values. Subsequently, we consider constraints on them from past measurements at LEP II on e^+e^- collisions into a pair of charged leptons plus missing energy and into a photon plus missing energy. These processes, respectively, receive contributions from the scotogenic reactions $e^+e^- \to H^+H^-$ and $e^+e^- \to \gamma NN', \gamma\mathcal{S}\mathcal{P}$ followed by the (sequential) decays of H, $N^{(\prime)}$, $\mathcal{S}$, and $\mathcal{P}$ into the DM particle N_1 plus light leptons. We show that the H^+H^- channel is subject to strict extra limitations from the LEP II data, whereas the neutral channels are not. Finally, we turn to the possibility of measuring the same e^+e^- scattering processes with higher energies and much improved precision at a future facility, in particular the ILC. We find that at the ILC such experiments can be expected to offer complementary information for probing the scotogenic model more extensively. Needless to say, future data on the Higgs boson's properties from the ILC will also be of great relevance to checking the model.

ACKNOWLEDGMENTS

This research was supported in part by the MOE Academic Excellence Program (Grant No. 102R891505) and the NCTS.

APPENDIX A: SOLUTIONS FOR YUKAWA COUPLINGS $\mathcal{Y}_{rk}$

The diagonalization relations in Eq. (14) can be exactly solved for the three pairs of Yukawa couplings $(Y_{ek}, Y_{\mu k})$, $k = 1, 2, 3$, in terms of $Y_k = Y_{\tau k}$. There are in total 27 sets

of the possible solutions. One can express the pairs in each set as $(Y_{ek}, Y_{\mu k}) = (\bar{e}_z, \bar{\mu}_z)Y_k$, where $z = a, b$, or c and

$$\bar{e}_a = \frac{-c_{12}c_{13}}{c_{12}c_{23}s_{13}e^{i\delta} - s_{12}s_{23}}, \quad \bar{\mu}_a = \frac{c_{12}s_{23}s_{13}e^{i\delta} + s_{12}c_{23}}{c_{12}c_{23}s_{13}e^{i\delta} - s_{12}s_{23}},$$
$$\bar{e}_b = \frac{-s_{12}c_{13}}{s_{12}c_{23}s_{13}e^{i\delta} + c_{12}s_{23}}, \quad \bar{\mu}_b = \frac{s_{12}s_{23}s_{13}e^{i\delta} - c_{12}c_{23}}{s_{12}c_{23}s_{13}e^{i\delta} + c_{12}s_{23}},$$
$$\bar{e}_c = \frac{s_{13}e^{-i\delta}}{c_{23}c_{13}}, \quad \bar{\mu}_c = \frac{s_{23}}{c_{23}}, \tag{A1}$$

with $c_{mn} = \cos\theta_{mn}$ and $s_{mn} = \sin\theta_{mn}$. Not all of the solution sets are desirable and lead to at least two nonzero masses among the eigenvalues $m_{1,2,3}$ in Eq. (14). Particularly, three of the sets can each only give one nonzero mass, while 18 (six) of the others can yield two (three) nonzero masses. We remark that the form of Eq. (9) also appears in some other models of radiative neutrino mass [27,30,33], and so these solutions for $Y_{\ell k}$ are also applicable to those models, with $\Lambda_{1,2,3}$ hiding the model details.

APPENDIX B: CROSS SECTIONS AND DECAY RATES

From the amplitude for $e^+(p_+)e^-(p_-) \to H^+H^-$ in Eq. (22), we arrive at the cross section

$$\sigma_{e\bar{e}\to H\bar{H}} = \frac{\pi\alpha^2\beta^3}{3s} + \frac{\alpha}{12}\frac{(g_L^2 + g_L g_R)\beta^3}{s - m_Z^2} + \frac{(g_L^4 + g_L^2 g_R^2)\beta^3 s}{96\pi(s - m_Z^2)} + \sum_k \frac{|\mathcal{Y}_{1k}|^4}{64\pi s}\left(w_k \ln\frac{w_k + \beta}{w_k - \beta} - 2\beta\right)$$
$$+ \left[\frac{\alpha}{16s} + \frac{g_L^2}{64\pi(s - m_Z^2)}\right]\sum_k |\mathcal{Y}_{1k}|^2\left[(w_k^2 - \beta^2)\ln\frac{w_k + \beta}{w_k - \beta} - 2\beta w_k\right]$$
$$+ \sum_{j,k>j} \frac{|\mathcal{Y}_{1j}\mathcal{Y}_{1k}|^2}{64\pi s}\left(\frac{w_j^2 - \beta^2}{w_j - w_k}\ln\frac{w_j + \beta}{w_j - \beta} + \frac{w_k^2 - \beta^2}{w_k - w_j}\ln\frac{w_k + \beta}{w_k - \beta} - 2\beta\right), \tag{B1}$$

where $s = (p_+ + p_-)^2$, we have assumed that s is not close to the Z pole, $j, k = 1, 2, 3$,

$$\alpha = \frac{e^2}{4\pi}, \quad \beta = \sqrt{1 - \frac{4m_H^2}{s}}, \quad w_k = 1 + \frac{2M_k^2}{s} - \frac{2m_H^2}{s} > \beta. \tag{B2}$$

We always take $e^\pm$ to be massless in our treatment of their scattering. The form of $\sigma_{e\bar{e}\to H\bar{H}}$ due to the γ- and Z-exchange diagrams plus a third contribution mediated by only one N has been known before in the literature [34]. In numerical computation of the e^+e^- collisions, we employ the effective values $\alpha = 1/128$, $g = 0.6517$, and $s_w^2 = 0.23146$ [3]. It is worth noting that in our examples of $\sigma_{e\bar{e}\to H\bar{H}}$ the N_k-mediated contributions tend to dominate the γ and Z diagrams, except in several instances where the different contributions are roughly comparable in size.

The neutral counterpart of the preceding transition is $e^+e^- \to \mathcal{SP}$, but it is generated at tree level by only one Z-exchange diagram. Its cross section is

$$\sigma_{e\bar{e}\to\mathcal{SP}} = \frac{(g_L - g_R)^2(g_L^2 + g_R^2)(s - 4m_0^2)^{3/2}}{96\pi\sqrt{s}(s - m_Z^2)^2} \tag{B3}$$

for $m_\mathcal{S} \simeq m_\mathcal{P} \simeq m_0$ and s away from the Z pole.

For the particle masses in our illustrations, $H^\pm$ and their neutral partners, $\mathcal{S}$ and $\mathcal{P}$, decay predominantly into the two-body final states $\ell_r^\pm N_k$ and νN_l, respectively, if kinematically permitted. From Eq. (6), we acquire their rates to be

$$\Gamma_{H\to\ell_r N_k} = \frac{|\mathcal{Y}_{rk}|^2}{16\pi m_H^3}(m_H^2 - m_{\ell_r}^2 - M_k^2)\sqrt{(m_H^2 - m_{\ell_r}^2 - M_k^2)^2 - 4m_{\ell_r}^2 M_k^2}, \tag{B4}$$

$$\Gamma_{\hat{\eta}\to\nu N_l} = \sum_r \frac{|\mathcal{Y}_{rl}|^2}{16\pi m_{\hat{\eta}}^3}(m_{\hat{\eta}}^2 - M_l^2)^2, \qquad \hat{\eta} = \mathcal{S} \quad \text{or} \quad \mathcal{P}. \tag{B5}$$

Therefore, for the total widths of $H^\pm$ and $\hat{\eta}$, we make the approximations $\Gamma_H = \sum_{r,k}\Gamma_{H\to\ell_r N_k}$ and $\Gamma_{\hat{\eta}} = \sum_k \Gamma_{\hat{\eta}\to\nu N_k}$ in our computation.

For the decays of N_k if $k = 2, 3$, the two-body modes $N_k \to \ell_r^{\pm} H^{\mp}$ and $N_k \to \nu\hat{\eta}$ may take place with rates

$$\Gamma_{N_k\to\ell_r^+H^-} = \Gamma_{N_k\to\ell_r^-H^+} = \frac{|\mathcal{Y}_{rk}|^2(M_k^2 + m_{\ell_r}^2 - m_H^2)}{32\pi M_k^3}\sqrt{(M_k^2 - m_{\ell_r}^2 - m_H^2)^2 - 4m_{\ell_r}^2 m_H^2},$$
$$\Gamma_{N_k\to\nu\hat{\eta}} = \sum_r \frac{|\mathcal{Y}_{rk}|^2}{32\pi M_k^3}(M_k^2 - m_{\hat{\eta}}^2)^2, \qquad \hat{\eta} = \mathcal{S} \quad \text{or} \quad \mathcal{P}. \tag{B6}$$

If these channels are closed, N_k will instead undergo $N_k \to \nu_o\nu_r N_l$ and possibly $N_k \to \ell_o^-\ell_r^+ N_l$, mediated by $\hat{\eta}$ and $H^{\pm}$, respectively. They lead to the combined rates

$$\Gamma_{N_k\to\nu\nu' N_l} = \frac{1}{2}\sum_{o,r}\Gamma_{N_k\to\nu_o\nu_r N_l}, \qquad \Gamma_{N_k\to\ell\bar{\ell}' N_l} = \sum_{o,r}\Gamma_{N_k\to\ell_o\bar{\ell}_r N_l}, \tag{B7}$$

where the factor of $1/2$ removes double counting of contributions with $o \neq r$ and accounts for identical Majorana neutrinos in final states with $o = r$. The terms in these sums are of the form

$$\Gamma_{N_k\to f_o(p_1)f_r(p_2)N_l(p_3)} = \frac{2}{(8\pi M_k)^3}\int d\bar{s}_{12}\, d\bar{s}_{23}\,\overline{|\mathcal{M}_{N_k\to f_o f_r N_l}|^2}, \tag{B8}$$

where $\bar{s}_{ik} = (p_i + p_k)^2$ and the expressions for the integrand are derived in the next paragraph. For the new particles' coupling and mass values which we have considered, these two- and/or three-body decay modes of N_k dominate its total width Γ_{N_k}.

Since ν and N are Majorana fermions, from Eq. (6), the amplitude for $N_k \to \nu_o(p_1)\nu_r(p_2)N_l(p_3)$ with $M_k < m_{\mathcal{S},\mathcal{P}}$ is

$$\begin{aligned}\mathcal{M}_{N_k\to\nu_o\nu_r N_l} = {}& \frac{-\bar{u}_{\nu_o}(\mathcal{Y}_{ok}P_R + \mathcal{Y}_{ok}^* P_L)u_{N_k}\bar{u}_{\nu_r}(\mathcal{Y}_{rl}P_R + \mathcal{Y}_{rl}^* P_L)v_{N_l}}{2\hat{\mathsf{s}}_{23}^{m_{\mathcal{S}}}} \\ & + \frac{\bar{u}_{\nu_o}(\mathcal{Y}_{ok}P_R - \mathcal{Y}_{ok}^* P_L)u_{N_k}\bar{u}_{\nu_r}(\mathcal{Y}_{rl}P_R - \mathcal{Y}_{rl}^* P_L)v_{N_l}}{2\hat{\mathsf{s}}_{23}^{m_{\mathcal{P}}}} \\ & + \frac{\bar{u}_{\nu_r}(\mathcal{Y}_{rk}P_R + \mathcal{Y}_{rk}^* P_L)u_{N_k}\bar{u}_{\nu_o}(\mathcal{Y}_{ol}P_R + \mathcal{Y}_{ol}^* P_L)v_{N_l}}{2\hat{\mathsf{s}}_{13}^{m_{\mathcal{S}}}} \\ & - \frac{\bar{u}_{\nu_r}(\mathcal{Y}_{rk}P_R - \mathcal{Y}_{rk}^* P_L)u_{N_k}\bar{u}_{\nu_o}(\mathcal{Y}_{ol}P_R - \mathcal{Y}_{ol}^* P_L)v_{N_l}}{2\hat{\mathsf{s}}_{13}^{m_{\mathcal{P}}}},\end{aligned} \tag{B9}$$

where

$$\hat{\mathsf{s}}_{ik}^m = \bar{s}_{ik} - m^2, \qquad \bar{s}_{ik} = (p_i + p_k)^2. \tag{B10}$$

Averaging (summing) the absolute square of this amplitude over initial (final) spins, we then get

$$\begin{aligned}\overline{|\mathcal{M}_{N_k\to\nu_o\nu_r N_l}|^2} = {}& -|\mathcal{Y}_{ok}\mathcal{Y}_{rl}|^2\frac{\hat{\mathsf{s}}_{23}^{M_k}\hat{\mathsf{s}}_{23}^{M_l}}{2}\left[\frac{1}{(\hat{\mathsf{s}}_{23}^{m_{\mathcal{S}}})^2} + \frac{1}{(\hat{\mathsf{s}}_{23}^{m_{\mathcal{P}}})^2}\right] - |\mathcal{Y}_{rk}\mathcal{Y}_{ol}|^2\frac{\hat{\mathsf{s}}_{13}^{M_k}\hat{\mathsf{s}}_{13}^{M_l}}{2}\left[\frac{1}{(\hat{\mathsf{s}}_{13}^{m_{\mathcal{S}}})^2} + \frac{1}{(\hat{\mathsf{s}}_{13}^{m_{\mathcal{P}}})^2}\right] \\ & + \mathrm{Re}(\mathcal{Y}_{ok}^*\mathcal{Y}_{rl}\mathcal{Y}_{rk}^*\mathcal{Y}_{ol})\frac{M_k M_l \bar{s}_{12}}{2}\left(\frac{1}{\hat{\mathsf{s}}_{23}^{m_{\mathcal{S}}}} + \frac{1}{\hat{\mathsf{s}}_{23}^{m_{\mathcal{P}}}}\right)\left(\frac{1}{\hat{\mathsf{s}}_{13}^{m_{\mathcal{S}}}} + \frac{1}{\hat{\mathsf{s}}_{13}^{m_{\mathcal{P}}}}\right) \\ & + \mathrm{Re}(\mathcal{Y}_{ok}^*\mathcal{Y}_{rl}^*\mathcal{Y}_{rk}\mathcal{Y}_{ol})\frac{M_k^2 M_l^2 - \bar{s}_{23}\bar{s}_{13}}{2}\left(\frac{1}{\hat{\mathsf{s}}_{23}^{m_{\mathcal{S}}}} - \frac{1}{\hat{\mathsf{s}}_{23}^{m_{\mathcal{P}}}}\right)\left(\frac{1}{\hat{\mathsf{s}}_{13}^{m_{\mathcal{S}}}} - \frac{1}{\hat{\mathsf{s}}_{13}^{m_{\mathcal{P}}}}\right).\end{aligned} \tag{B11}$$

Similarly, the amplitude for $N_k \to \ell_o^-(p_1)\ell_r^+(p_2)N_l(p_3)$ with $M_k < m_H + m_{\ell_o,\ell_r}$ is

$$\mathcal{M}_{N_k\to\ell_o\bar{\ell}_r N_l} = \frac{\mathcal{Y}_{ok}\mathcal{Y}_{rl}^*\bar{u}_{\ell_o}P_R u_{N_k}\bar{u}_{N_l}P_L v_{\ell_r}}{\hat{\mathsf{s}}_{23}^{m_H}} - \frac{\mathcal{Y}_{rk}^*\mathcal{Y}_{ol}\bar{u}_{N_l}\gamma^\lambda P_L u_{N_k}\bar{u}_{\ell_o}\gamma_\lambda P_L v_{\ell_r}}{2\hat{\mathsf{s}}_{13}^{m_H}}, \tag{B12}$$

leading to

$$\overline{|\mathcal{M}_{N_k\to\ell_o\bar{\ell}_r N_l}|^2} = -|\mathcal{Y}_{ok}\mathcal{Y}_{rl}|^2\frac{(\hat{\mathsf{s}}_{23}^{M_k}-m_{\ell_o}^2)(\hat{\mathsf{s}}_{23}^{M_l}-m_{\ell_r}^2)}{2(\hat{\mathsf{s}}_{23}^{m_H})^2} - |\mathcal{Y}_{rk}\mathcal{Y}_{ol}|^2\frac{(\hat{\mathsf{s}}_{13}^{M_k}-m_{\ell_r}^2)(\hat{\mathsf{s}}_{13}^{M_l}-m_{\ell_o}^2)}{2(\hat{\mathsf{s}}_{13}^{m_H})^2} + \mathrm{Re}(\mathcal{Y}_{ok}^*\mathcal{Y}_{rl}\mathcal{Y}_{rk}^*\mathcal{Y}_{ol})\frac{M_kM_l(\bar{s}_{12}-m_{\ell_o}^2-m_{\ell_r}^2)}{\hat{\mathsf{s}}_{23}^{m_H}\hat{\mathsf{s}}_{13}^{m_H}}. \tag{B13}$$

In the case of $m_0 \simeq m_{\mathcal{S}} \simeq m_{\mathcal{P}}$, the formulas in this paragraph are related by crossing symmetry to those for $N_kN_l \to \nu_o\nu_r$ and $N_kN_l \to \ell_o^-\ell_r^+$ given in Ref. [6].[8]

For the scattering $e^+(p_+)e^-(p_-)\to\gamma(K)N_k(q_-)N_l(q_+)$, one can define the Lorentz-invariant kinematical variables

$$\begin{aligned} &s=(p_++p_-)^2, \quad s'=(q_++q_-)^2, \quad t=(p_+-q_+)^2, \quad t'=(p_--q_-)^2,\\ &u=(p_+-q_-)^2, \quad u'=(p_--q_+)^2, \quad \kappa_\pm=2K\cdot p_\pm, \quad \kappa'_\pm=2K\cdot q_\pm, \end{aligned} \tag{B14}$$

before deriving its amplitude $\mathcal{M}_{e\bar{e}\to\gamma N_kN_l}$. Because of the Majorana nature of $N_{k,l}$, at tree level the amplitude comes from six diagrams mediated by H with the photon radiated from the $e^\pm$ legs and the H lines. We write it as

$$\begin{aligned} \mathcal{M}_{e\bar{e}\to\gamma N_kN_l} = e\mathcal{Y}_{1k}^*\mathcal{Y}_{1l}\Big\{&\frac{\bar{u}_{N_k}P_L(\not{p}_- - \not{K})\not{\varepsilon}^* u_{e^-}\bar{v}_{e^+}P_Rv_{N_l}}{(t-m_H^2)\kappa_-} - \frac{\bar{u}_{N_k}P_Lu_{e^-}\bar{v}_{e^+}\not{\varepsilon}^*(\not{p}_+ - \not{K})P_Rv_{N_l}}{(t'-m_H^2)\kappa_+}\\ &- \frac{2\bar{u}_{N_k}P_Lu_{e^-}\bar{v}_{e^+}P_Rv_{N_l}\varepsilon^*\cdot(p_--q_-)}{(t-m_H^2)(t'-m_H^2)}\Big\} + e\mathcal{Y}_{1k}\mathcal{Y}_{1l}^*\Big\{\frac{\bar{u}_{N_k}\gamma^\rho P_Lv_{N_l}\bar{v}_{e^+}\gamma_\rho P_L(\not{p}_- - \not{K})\not{\varepsilon}^*u_{e^-}}{2(m_H^2-u)\kappa_-}\\ &- \frac{\bar{u}_{N_k}\gamma^\rho P_Lv_{\bar{N}}\bar{v}_{e^+}\not{\varepsilon}^*(\not{p}_+ - \not{K})\gamma_\rho P_Lu_{e^-}}{2(m_H^2-u')\kappa_+} + \frac{\bar{u}_{N_k}\gamma^\rho P_Lv_{N_l}\bar{v}_{e^+}\gamma_\rho P_Lu_{e^-}\varepsilon^*\cdot(p_--q_+)}{(u-m_H^2)(u'-m_H^2)}\Big\}. \end{aligned} \tag{B15}$$

It is straightforward to check that this amplitude respects electromagnetic gauge invariance. Averaging (summing) the absolute square of $\mathcal{M}_{e\bar{e}\to\gamma N_kN_l}$ over the initial (final) spins, one then obtains

$$\begin{aligned} \frac{\overline{|\mathcal{M}_{e\bar{e}\to\gamma N_kN_l}|^2}}{e^2} = &\frac{|\mathcal{Y}_{1k}\mathcal{Y}_{1l}|^2}{2\kappa_-}\Big\{\frac{M_l^2-t}{(m_H^2-t)^2}\Big[\kappa'_- + \frac{(M_k^2+t')\kappa_- + 2(M_k^2-t)(M_k^2-t')}{m_H^2-t'} - \frac{(M_k^2-t')(t+t')\kappa_-}{2(m_H^2-t')^2}\Big]\\ &+ \frac{M_k^2-u}{(m_H^2-u)^2}\Big[\kappa'_+ + \frac{(M_l^2+u')\kappa_- + 2(M_l^2-u)(M_l^2-u')}{m_H^2-u'} - \frac{(M_l^2-u')(u+u')\kappa_-}{2(m_H^2-u')^2}\Big]\\ &+ \frac{(M_l^2-t)[(t'-s-u)\kappa_- + (M_k^2-t)s] + (M_k^2-t')[(t-s-u')\kappa_+ + (M_l^2-t')s]}{2(m_H^2-t)(m_H^2-t')\kappa_+}\\ &+ \frac{(M_k^2-u)[(u'-s-t)\kappa_- + (M_l^2-u)s] + (M_l^2-u')[(u-s-t')\kappa_+ + (M_k^2-u')s]}{2(m_H^2-u)(m_H^2-u')\kappa_+}\Big\}\\ &- \frac{M_kM_l\,\mathrm{Re}(\mathcal{Y}_{1k}^{*2}\mathcal{Y}_{1l}^2)}{(m_H^2-t)(m_H^2-u)\kappa_-}\Big[\kappa_+ + \frac{(m_H^2-u)ss'}{(m_H^2-u')\kappa_+} + \frac{(2M_k^2+2M_l^2+s-s')\kappa_-s}{4(m_H^2-t')(m_H^2-u')}\\ &+ \frac{(M_k^2-u)\kappa_- - (M_k^2-t')\kappa_+ + (2M_k^2-t-t')s}{2(m_H^2-t')} + \frac{(M_l^2-t)\kappa_- - (M_l^2-u')\kappa_+ + (2M_l^2-u-u')s}{2(m_H^2-u')}\Big]\\ &+ \frac{4M_kM_l\,\mathrm{Re}(\mathcal{Y}_{1k}^*\mathcal{Y}_{1l})\,\mathrm{Im}(\mathcal{Y}_{1k}^*\mathcal{Y}_{1l})}{(m_H^2-t)(m_H^2-u)\kappa_-}\left(\frac{1}{m_H^2-t'}+\frac{1}{m_H^2-u'}\right)\epsilon_{\rho\sigma\tau\omega}p_+^\rho p_-^\sigma q_+^\tau q_-^\omega\\ &+ \left(t\leftrightarrow t', u\leftrightarrow u', \kappa_-\leftrightarrow\kappa_+, \kappa'_-\leftrightarrow\kappa'_+, M_k\leftrightarrow M_l, \mathcal{Y}_{1k}\leftrightarrow\mathcal{Y}_{1l}\right). \end{aligned} \tag{B16}$$

This leads to the cross section

[8]The expression for $\overline{|\mathcal{M}_{N_kN_l\to\nu_i\nu_j}|^2}$ in Eq. (B3) of Ref. [6] needs to be multiplied by an overall factor of 2 due to $\nu_{i,j}$ being Majorana particles. Since the final neutrinos are not observed, the corresponding cross section is $\sigma_{N_kN_l\to\nu\nu'} = (1/2)\sum_{i,j}\sigma_{N_kN_l\to\nu_i\nu_j}$, where the factor of $1/2$ removes double counting of contributions with $i\neq j$ and accounts for identical neutrinos in final states with $i=j$. As a consequence, the results in Ref. [6] for the DM annihilation $N_1N_1\to\nu\nu', \ell\bar{\ell}'$ are numerically unaffected.

$$\sigma_{e\bar{e}\to\gamma N_k N_l} = \int \frac{E_\gamma dE_\gamma d(\cos\theta_\gamma) d\bar{\Omega}_N}{2(1+\delta_{kl})(4\pi)^4 s} \sqrt{1 - \frac{2M_k^2 + 2M_l^2}{s - 2E_\gamma\sqrt{s}} + \left(\frac{M_k^2 - M_l^2}{s - 2E_\gamma\sqrt{s}}\right)^2}\, \overline{|\mathcal{M}_{e\bar{e}\to\gamma N_k N_l}|^2}, \tag{B17}$$

where E_γ and θ_γ are the photon energy and angle with respect to the e^+ or e^- beam direction in the c.m. frame of the e^+e^- pair, $\bar{\Omega}_N$ denotes the solid angle of either N_k or N_l in the c.m. frame of the $N_k N_l$ pair, and the factor $1/(1+\delta_{kl})$ accounts for the identical Majorana fermions in the final states with $k = l$. The range of the photon energy is

$$E_\gamma^{\min} \le E_\gamma \le E_\gamma^{\max} = \frac{s - (M_k + M_l)^2}{2\sqrt{s}}, \tag{B18}$$

where $E_\gamma^{\min}$ is an experimental cut. In the numerical evaluation of the integral, the θ_γ range is also subject to cuts.

For $e^+(p_+)e^-(p_-) \to \gamma(K)\mathcal{S}(q_-)\mathcal{P}(q_+)$, the kinematical variables are the same as those listed in Eq. (B14). This reaction is induced at tree level by two Z-exchange diagrams with the photon emitted from the $e^\pm$ lines. Its amplitude is

$$\begin{aligned}\mathcal{M}_{e\bar{e}\to\gamma\mathcal{S}\mathcal{P}} = {} & \frac{2ie\bar{v}_{e^+}\not{q}_-[(g_L g_R - g_L^2)P_L + (g_R^2 - g_L g_R)P_R](\not{p}_- - \not{K})\not{\epsilon}^* u_{e^-}}{(s' - m_Z^2 + i\Gamma_Z m_Z)\kappa_-} \\ & + \frac{2ie\bar{v}_{e^+}\not{\epsilon}^*(\not{K} - \not{p}_+)\not{q}_-[(g_L g_R - g_L^2)P_L + (g_R^2 - g_L g_R)P_R]u_{e^-}}{(s' - m_Z^2 + i\Gamma_Z m_Z)\kappa_+},\end{aligned} \tag{B19}$$

where $g_{L,R}$ are defined in Sec. IV B. One can easily verify that $\mathcal{M}_{e\bar{e}\to\gamma\mathcal{S}\mathcal{P}}$ is electromagnetically gauge invariant. It follows that

$$\sigma_{e\bar{e}\to\gamma\mathcal{S}\mathcal{P}} = \int \frac{E_\gamma dE_\gamma d(\cos\theta_\gamma) d\bar{\Omega}_{\hat{\eta}}}{2(4\pi)^4 s} \sqrt{1 - \frac{4m_0^2}{s - 2E_\gamma\sqrt{s}}}\, \overline{|\mathcal{M}_{e\bar{e}\to\gamma\mathcal{S}\mathcal{P}}|^2}, \tag{B20}$$

where $\bar{\Omega}_{\hat{\eta}}$ denotes the solid angle of either $\mathcal{S}$ or $\mathcal{P}$ in the c.m. frame of the $\mathcal{S}\mathcal{P}$ pair and

$$\overline{|\mathcal{M}_{e\bar{e}\to\gamma\mathcal{S}\mathcal{P}}|^2} = 2e^2(g_L - g_R)^2(g_L^2 + g_R^2)\frac{s'(tu + t'u' + m_0^2 s - 2m_0^4) + m_0^2(2\kappa_+\kappa_- - s^2)}{\kappa_+\kappa_-[(s' - m_Z^2)^2 + \Gamma_Z^2 m_Z^2]}. \tag{B21}$$

The photon energy range in this case is

$$E_\gamma^{\min} \le E_\gamma \le E_\gamma^{\max} = \frac{s - 4m_0^2}{2\sqrt{s}}. \tag{B22}$$

Finally, it is instructive to compare our calculation of $\sigma_{e\bar{e}\to\gamma N_k N_l, \gamma\mathcal{S}\mathcal{P}}$ above with its estimation in the so-called radiator approximation [35]. For $XY = N_k N_l$ or $\mathcal{S}\mathcal{P}$, it is given by

$$\begin{aligned}\sigma_{e\bar{e}\to\gamma XY} &\simeq \int dc_\gamma dx_\gamma \mathcal{H}(c_\gamma, x_\gamma; s)\hat{\sigma}(\hat{s}), \qquad c_\gamma = \cos\theta_\gamma, \qquad x_\gamma = \frac{2E_\gamma}{\sqrt{s}}, \\ \mathcal{H}(c, x; s) &= \frac{\alpha}{\pi}\frac{(2-x)^2 + c^2x^2}{2(1-c^2)x}, \qquad \hat{s} = (1 - x_\gamma)s,\end{aligned} \tag{B23}$$

where $\hat{\sigma}(\hat{s})$ denotes the cross section of the simpler reaction $e^+e^- \to XY$. Thus we acquire numbers which are smaller than their counterparts in Table III by less than 9%. In contrast, our application of this approximate method to $\sigma^{\rm SM}_{e^+e^-\to\gamma\nu\bar{\nu}}$, with $\hat{\sigma}(\hat{s})$ now being the SM cross section of $e^+e^- \to \nu\bar{\nu}$, works as well only for the $\sqrt{s} = 250$ GeV case, its result exceeding the corresponding number in the bottom row of Table III by about 9%, whereas the estimates for $\sqrt{s} = 500, 1000$ GeV overshoot their counterparts in the table by more than 100%.

[1] G. Aad *et al.* (ATLAS Collaboration), Phys. Lett. B **716**, 1 (2012); S. Chatrchyan *et al.* (CMS Collaboration), Phys. Lett. B **716**, 30 (2012); http://press.web.cern.ch/press-releases/2013/03/new-results-indicate-particle-discovered-cern-higgs-boson.

[2] F. P. An *et al.* (DAYA-BAY Collaboration), Phys. Rev. Lett. **108**, 171803 (2012); J. K. Ahn *et al.* (RENO Collaboration), Phys. Rev. Lett. **108**, 191802 (2012).

[3] J. Beringer *et al.* (Particle Data Group Collaboration), Phys. Rev. D **86**, 010001 (2012).

[4] P. A. R. Ade *et al.* (Planck Collaboration), arXiv:1303.5062.

[5] E. Ma, Phys. Rev. D **73**, 077301 (2006).

[6] S. Y. Ho and J. Tandean, Phys. Rev. D **87**, 095015 (2013).

[7] A. Heister *et al.* (ALEPH Collaboration), Eur. Phys. J. C **38**, 147 (2004); J. Abdallah *et al.* (DELPHI Collaboration), Eur. Phys. J. C **34**, 127 (2004); P. Achard *et al.* (L3 Collaboration), Phys. Lett. B **600**, 22 (2004); G. Abbiendi *et al.* (OPAL Collaboration), Eur. Phys. J. C **52**, 767 (2007).

[8] D. Buskulic *et al.* (ALEPH Collaboration), Phys. Lett. B **384**, 333 (1996); R. Barate *et al.* (ALEPH Collaboration), Phys. Lett. B **420**, 127 (1998); R. Barate *et al.* (ALEPH Collaboration), Phys. Lett. B **429**, 201 (1998); A. Heister *et al.* (ALEPH Collaboration), Eur. Phys. J. C **28**, 1 (2003); P. Abreu *et al.* (DELPHI Collaboration), Eur. Phys. J. C **17**, 53 (2000); J. Abdallah *et al.* (DELPHI Collaboration), Eur. Phys. J. C **38**, 395 (2005); M. Acciarri *et al.* (L3 Collaboration), Phys. Lett. B **415**, 299 (1997); M. Acciarri *et al.* (L3 Collaboration), Phys. Lett. B **444**, 503 (1998); M. Acciarri *et al.* (L3 Collaboration), Phys. Lett. B **470**, 268 (1999); K. Ackerstaff *et al.* (OPAL Collaboration), Eur. Phys. J. C **2**, 607 (1998); G. Abbiendi *et al.* (OPAL Collaboration), Eur. Phys. J. C **8**, 23 (1999); G. Abbiendi *et al.* (OPAL Collaboration), Eur. Phys. J. C **18**, 253 (2000).

[9] T. Behnke *et al.*, arXiv:1306.6327.

[10] The one-loop renormalization of this model has been investigated in R. Bouchand and A. Merle, J. High Energy Phys. 07 (2012) 084.

[11] J. Kubo, E. Ma, and D. Suematsu, Phys. Lett. B **642**, 18 (2006); D. Suematsu, T. Toma, and T. Yoshida, Phys. Rev. D **79**, 093004 (2009); D. Schmidt, T. Schwetz, and T. Toma, Phys. Rev. D **85**, 073009 (2012).

[12] B. Pontecorvo, Zh. Eksp. Teor. Fiz. **53** (1968) 1717 [Sov. Phys. JETP **26**, 984 (1968)]; Z. Maki, M. Nakagawa, and S. Sakata, Prog. Theor. Phys. **28**, 870 (1962).

[13] M. C. Gonzalez-Garcia, M. Maltoni, J. Salvado, and T. Schwetz, J. High Energy Phys. 12 (2012) 123.

[14] D. V. Forero, M. Tortola, and J. W. F. Valle, Phys. Rev. D **86**, 073012 (2012); G. L. Fogli, E. Lisi, A. Marrone, D. Montanino, A. Palazzo, and A. M. Rotunno, Phys. Rev. D **86**, 013012 (2012).

[15] P. F. Harrison, D. H. Perkins, and W. G. Scott, Phys. Lett. B **530**, 167 (2002); Z. Z. Xing, Phys. Lett. B **533**, 85 (2002); X. G. He and A. Zee, Phys. Lett. B **560**, 87 (2003).

[16] S. Kashiwase and D. Suematsu, Eur. Phys. J. C **73**, 2484 (2013).

[17] G. Aad *et al.* (ATLAS Collaboration), Phys. Lett. B **726**, 88 (2013).

[18] CMS Collaboration, Report No. CMS-PAS-HIG-13-005, 2013 (unpublished).

[19] S. Heinemeyer *et al.* (LHC Higgs Cross Section Working Group Collaboration), arXiv:1307.1347.

[20] N. G. Deshpande and E. Ma, Phys. Rev. D **18**, 2574 (1978).

[21] ATLAS Collaboration, Report No. ATLAS-CONF-2013-009, 2013 (unpublished); S. Chatrchyan *et al.* (CMS Collaboration), Phys. Lett. B **726**, 587 (2013).

[22] K. Cheung, J. S. Lee, and P. Y. Tseng, J. High Energy Phys. 05 (2013) 134; A. Falkowski, F. Riva, and A. Urbano, J. High Energy Phys. 11 (2013) 111; P. P. Giardino, K. Kannike, I. Masina, M. Raidal, and A. Strumia, J. High Energy Phys. 05 (2014) 046; J. Ellis and T. You, J. High Energy Phys. 06 (2013) 103.

[23] R. Barbieri, L. J. Hall, and V. S. Rychkov, Phys. Rev. D **74**, 015007 (2006); Q. H. Cao, E. Ma, and G. Rajasekaran, Phys. Rev. D **76**, 095011 (2007).

[24] M. Aoki, S. Kanemura, and H. Yokoya, Phys. Lett. B **725**, 302 (2013).

[25] See, e.g., E. Ma, and J. Okada, Phys. Rev. D **18**, 4219 (1978); A. Birkedal, K. Matchev, and M. Perelstein, Phys. Rev. D **70**, 077701 (2004).

[26] See, e.g., P. Konar, K. Kong, K. T. Matchev, and M. Perelstein, New J. Phys. **11**, 105004 (2009); C. Bartels, M. Berggren, and J. List, Eur. Phys. J. C **72**, 2213 (2012).

[27] C. Boehm, Y. Farzan, T. Hambye, S. Palomares-Ruiz, and S. Pascoli, Phys. Rev. D **77**, 043516 (2008); Y. Farzan, Phys. Rev. D **80**, 073009 (2009); Mod. Phys. Lett. A **25**, 2111 (2010).

[28] Y. Farzan and M. Hashemi, J. High Energy Phys. 11 (2010) 029.

[29] C. W. Chiang, G. Faisel, Y. F. Lin, and J. Tandean, J. High Energy Phys. 10 (2013) 150.

[30] A. Ahriche and S. Nasri, J. Cosmol. Astropart. Phys. 07 (2013) 035.

[31] S. S. C. Law and K. L. McDonald, J. High Energy Phys. 09 (2013) 092.

[32] E. Ma and J. Okada, Phys. Rev. Lett. **41**, 287 (1978); **41**, 1759E (1978); K. J. F. Gaemers, R. Gastmans, and F. M. Renard, Phys. Rev. D **19**, 1605 (1979); F. A. Berends, G. J. H. Burgers, C. Mana, M. Martinez, and W. L. van Neerven, Nucl. Phys. **B301**, 583 (1988).

[33] G. Guo, X. G. He, and G. N. Li, J. High Energy Phys. 10 (2012) 044; G. N. Li, G. Guo, B. Ren, Y. J. Zheng, and X. G. He, J. High Energy Phys. 04 (2013) 026.

[34] S. Komamiya, Phys. Rev. D **38**, 2158 (1988); D. Atwood, S. Bar-Shalom, and A. Soni, Phys. Rev. D **76**, 033004 (2007).

[35] O. Nicrosini and L. Trentadue, Nucl. Phys. **B318**, 1 (1989); G. Montagna, O. Nicrosini, F. Piccinini, and L. Trentadue, Nucl. Phys. **B452**, 161 (1995).